

Li ion migration in Li₃PO₄ electrolytes: Effects of O vacancies and N substitutions

Y. A. Du^a and N. A. W. Holzwarth^a

^a Department of Physics, Wake Forest University,
Winston-Salem, North Carolina 27106, USA

Motivated by recent developments in solid electrolytes based on lithium phosphorous oxynitride (LiPON) materials, we carried out computer simulations in order to develop an understanding of the detailed mechanisms of ionic transport. Starting with crystalline Li₃PO₄, we investigated some possible structures of isolated defects associated with extrinsic Li ion vacancies and interstitials. In particular, we identified a “PNP” structure which involves a bridging N between two phosphate groups, formed from the combination of an O vacancy and a N substitution, stabilizing a Li ion vacancy. We also studied the effects of N substituting for a tetrahedral O in a phosphate group which stabilizes a Li interstitial ion. In addition to studying the structures of these isolated defects as sources of extrinsic mobile Li ions, we also modeled their effects on the mobilities of the ions.

Introduction

Lithium phosphorous oxynitride (LiPON) films are under development at Oak Ridge National Laboratory (1–4) as very promising solid state electrolytes for use in rechargeable batteries and other applications. These LiPON films have variable composition which can be quantified as Li_{3+x}PO_{4-y}N_z, where $x=3z-2y$ for neutral systems. Depending on composition, activation energies for Li ion conductivity have been reported in the literature in the range of 0.4 eV ≤ E_A ≤ 0.7 eV. (1–6) In addition to having good Li ion conductivity, the films have excellent chemical and physical stability in general and, more importantly, at their interfaces with cathodes and anodes.

The purpose of this work is to use first-principles modeling techniques to help develop an understanding of detailed mechanisms of Li ion migration in these materials. In previous work, (7) we used first-principles calculations to model Li ion migration in crystalline Li₃PO₄, finding very good agreement with the experimental measurements. In the present work, we used the same methods to study the effects of O vacancies and N substitutions on migration energies of Li ion vacancies and interstitials as a first step towards understanding Li ion migration in the disordered LiPON films.

For comparison with experiment, the temperature (T) dependence of the ionic conductivity σ in terms of the Arrhenius relation

$$\sigma \cdot T = K e^{-E_A/kT} \quad [1]$$

quantifies the activation energy E_A of the process which is determined in our simulations. Here k denotes the Boltzmann constant, K denotes a temperature independent constant.

Table I summarizes some of the experimentally determined values of activation energies in these materials showing that both stoichiometry and structure are important for controlling the ionic conductivity.

Table I: Activation energies measured in Li phosphate materials

Material	Reference	E_A (eV)
Polycrystalline γ -Li ₃ PO ₄	3	1.24
Polycrystalline Li _{2.88} PO _{3.73} N _{0.14}	3	0.97
LiPON thin films	1-6	0.4-0.7

While our simulations are not yet able to model disordered materials, we can learn a good deal by studies based on the crystalline materials. In this work, we have investigated some possible structures of isolated defects associated with extrinsic Li ion vacancies and interstitials. We identified some structures involving bridging N or O between two phosphate groups which result from the removal an O and which stabilize a Li vacancy. We also studied the effects of N substituting for a tetrahedral O in a phosphate group which stabilizes a Li interstitial ion. In addition to studying the structures of these isolated defects as sources of extrinsic mobile Li ions, we also considered their effects on the mobility of the ions. We are able to use these results to infer some properties of the disordered LiPON material.

Computational Methods

The calculational methods used in the present work were the same as reported in our previous studies of intrinsic Li ion mobility in crystalline Li₃PO₄. (7) In particular, the calculations are based on density functional theory (8) and use the local density approximation for the exchange-correlation functional. (9) The calculations were carried out using the Quantum Espresso (PWSCF) package (10) with the ultrasoft pseudopotential formalism. (11) Estimates of the migration energies E_m for the Li ion diffusion were calculated using the nudged elastic band (NEB) method (12-14) as implemented in the PWSCF code. Most of the defect structures were based on 128 atom supercells of the perfect crystal using the same lattice parameters optimized in our previous work.

Results for Li ion migration in crystalline γ -Li₃PO₄

Table II summarizes calculated and measured results for Li ion migration in crystalline γ -Li₃PO₄, where we considered both vacancy and interstitial Li ion migration paths along the 3 crystallographic directions. We find that the interstitial Li ion migration through an interstitialcy mechanism has lower migration energy than vacancy migration through a direct hopping mechanism. In the ideal crystal there are no intrinsic Li ions so that the activation energy for Li ion conductivity is determined by the combination of the “formation” energy E_f needed to produce a mobile Li ion by means of a vacancy-interstitial pair in addition to the migration energy E_m with the relation $E_A = E_m + E_f / 2$. Using these results with the estimated formation energy, we find excellent agreement with the conductivity measurements for the single crystal (15) as well as with the

polycrystalline measurements mentioned in Table I. This analysis indicates that for crystalline Li_3PO_4 , the activation energy is large because of the bottleneck of producing the intrinsic mobile ions and that the interstitialcy mechanism is mostly responsible for ionic transport.

Table II: Activation energies for Li ion migration in $\gamma\text{-Li}_3\text{PO}_4$

Axis	E_m	$E_A = E_m + E_f/2$ (calc) ^a	E_A (exp) ^b
a (vacancy)	0.7 eV	1.5 eV	1.23 eV
a (interstitial)	0.4 eV	1.3 eV	
b (vacancy)	0.7 eV	1.6 eV	1.14 eV
b (interstitial)	0.3 eV	1.1 eV	
c (vacancy)	0.7 eV	1.5 eV	1.14 eV
c (interstitial)	0.3 eV	1.1 eV	

^aRef. 7. ^bRef. 15.

Simulation of defects which stabilize Li ion vacancies

One way to avoid the formation energy bottleneck is to dope the crystal and produce extrinsic mobile Li ions so that the activation in Eq. [1] is determined by the migration energy alone: $E_A = E_m$. We first consider the production of Li ion vacancies. In these materials, Li ion vacancies are most conveniently stabilized by removing O. Motivated by experimental studies on the LiPON materials, (1-6) we studied supercells based on the stoichiometry $\text{Li}_{3-1/16}\text{PO}_{4-2/16}\text{N}_{1/16}$ in which for every 16 formula units of Li_3PO_4 one oxygen ion is removed, another is replaced with nitrogen, and one Li ion is removed. For this stoichiometry, there are many possible defect structures. We found two geometries in which the removal of the O ion resulted in rebonding the phosphate ions to form $\text{O}_3\text{P}-\text{O}-\text{PO}_3$ groups. The structures could be further stabilized by replacing the “bridging” $-\text{O}-$ unit with a “bridging” $-\text{N}-$ unit to form $\text{O}_3\text{P}-\text{N}-\text{PO}_3$ or “PNP” structures. Depending on which of the 3 inequivalent O sites of the original $\gamma\text{-Li}_3\text{PO}_4$ are removed, the PNP structure can be either “bent” or “straight” as shown in Fig. 1 below.

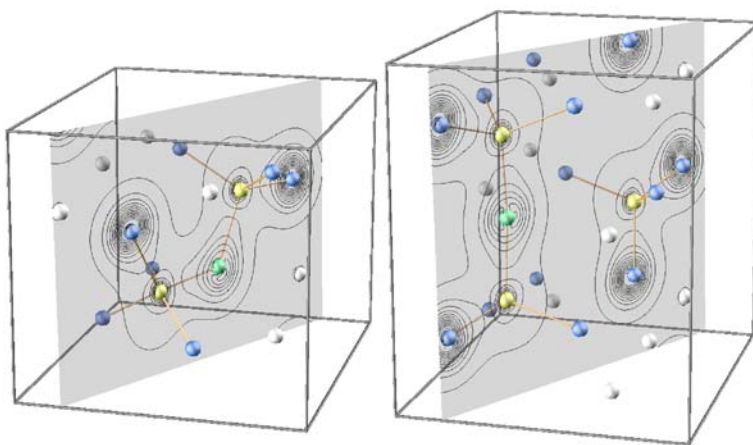


Figure 1. Diagrams of bent (left) and straight (right) PNP structures. Li ions are denoted with light unbonded spheres. The PO_4 and $\text{O}_3\text{P}-\text{N}-\text{PO}_3$ structures are indicated with smaller bonded spheres. Contour plots of the valence electron densities are plotted in the PNP planes.

The lengths of the “bridging” bonds were found to be 1.6—1.7 Å while the typical bond P—O bond length in a tetrahedral PO₄ unit is 1.5 Å. The bond angle of the “bent” PNP structure is approximately 120°, while that of the “straight” PNP structure is approximately 175°. The density of states of this defect structure is shown in Fig. 2 in comparison with that of the crystalline γ -Li₃PO₄. Here we see that the bridging —N— bonds contributes a low energy state below the valence band of the crystal. This state corresponds to N 2p σ orbitals whose lower energy can be understood in terms of the electrostatic energy introduced by the two nearby P ions. In fact, the partial density of states corresponding to O sites “associated” with the O₃P—N—PO₃ structure are also lowered in energy due to the electrostatic energy of the P ions as shown in the plot. The PNP defect also has a contribution from N 2p π orbitals at the top of the valence band which is a consequence of the smaller binding energy of the N nucleus compared to that of O. The density of states plot for the “straight” PNP defect is similar.

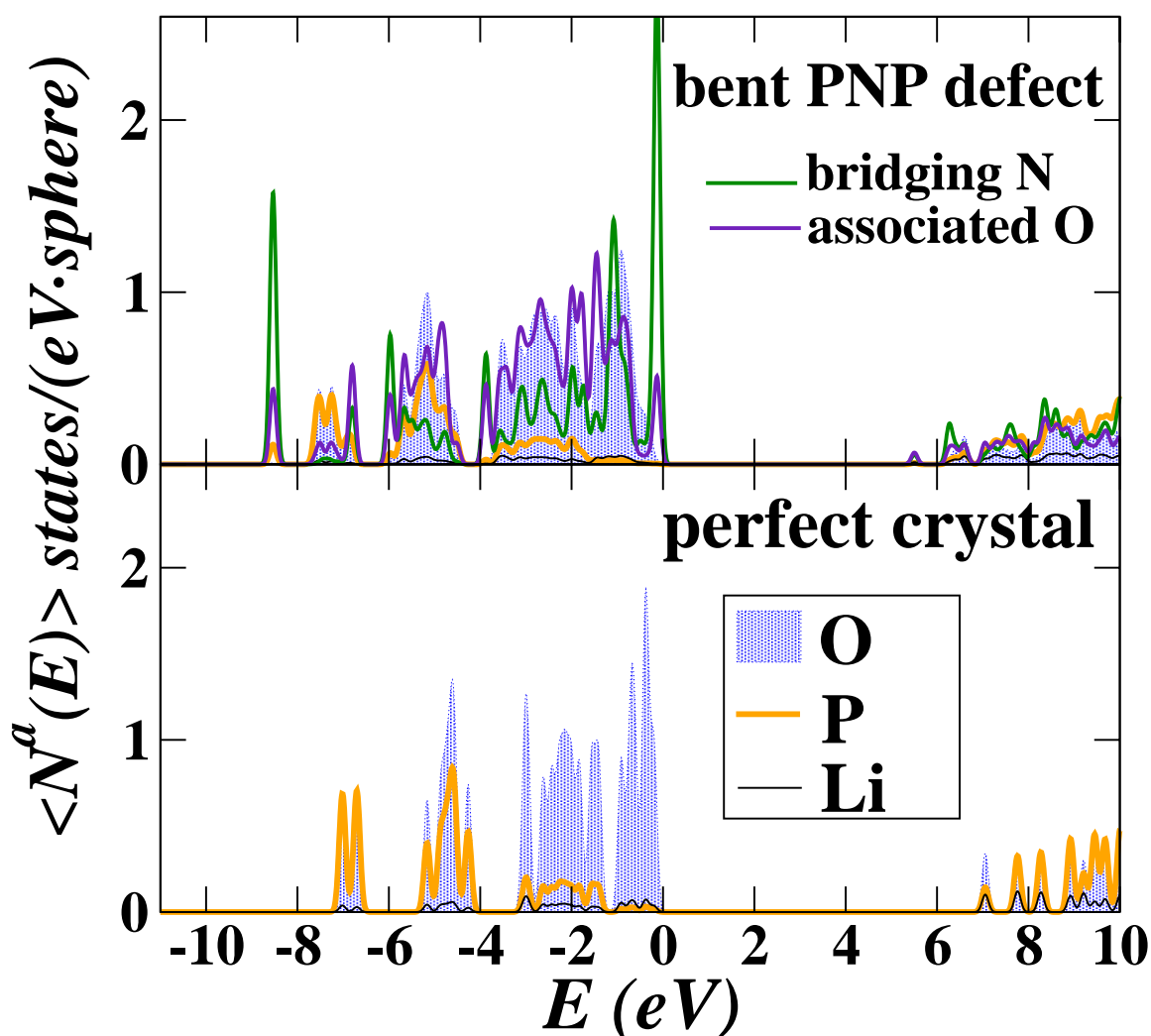


Figure 2. Plot of partial densities of states for bent PNP defect in the $\text{Li}_{3-1/16}\text{PO}_{4-2/16}\text{N}_{1/16}$ supercell (top) compared with that of γ -Li₃PO₄ in the same supercell (bottom). The partial densities of states are weighted by the charge within spheres surrounding each indicated atom type, averaged over all spheres of that type.

From the identification of these PNP structures as likely sources for extrinsic Li ion vacancies, the next question is how they affect the migration energies E_m . We have identified several metastable configurations of the Li ion vacancy in these materials. While the PNP structure (bond angles and bond lengths) are insensitive to the vacancy position, the energy of the system increases by as much as 0.8 eV as the vacancy moves far from the PNP structure. For estimating the migration energies E_m , we have simulated several hopping steps between these metastable Li ion vacancy configurations using the NEB method. An example of migration along the **b**-axis of the crystal is shown below in Fig. 3. We see that site 1, which is closest to the defect, has an energy of between -0.7 and -0.8 eV relative to sites 2-4 for which the environment is similar to that of the bulk crystal. In this sense, the PNP defect is seen to provide a “trap” for the Li ion vacancy. The migration energy for the vacancy moving from site 1 to 2 is 1 eV while the overall migration for vacancy motion along the **b**-axis is 1.5 eV. The migration energies for selected vacancy diffusion steps calculated along different crystallographic axes are summarized in Table III in the summary section.

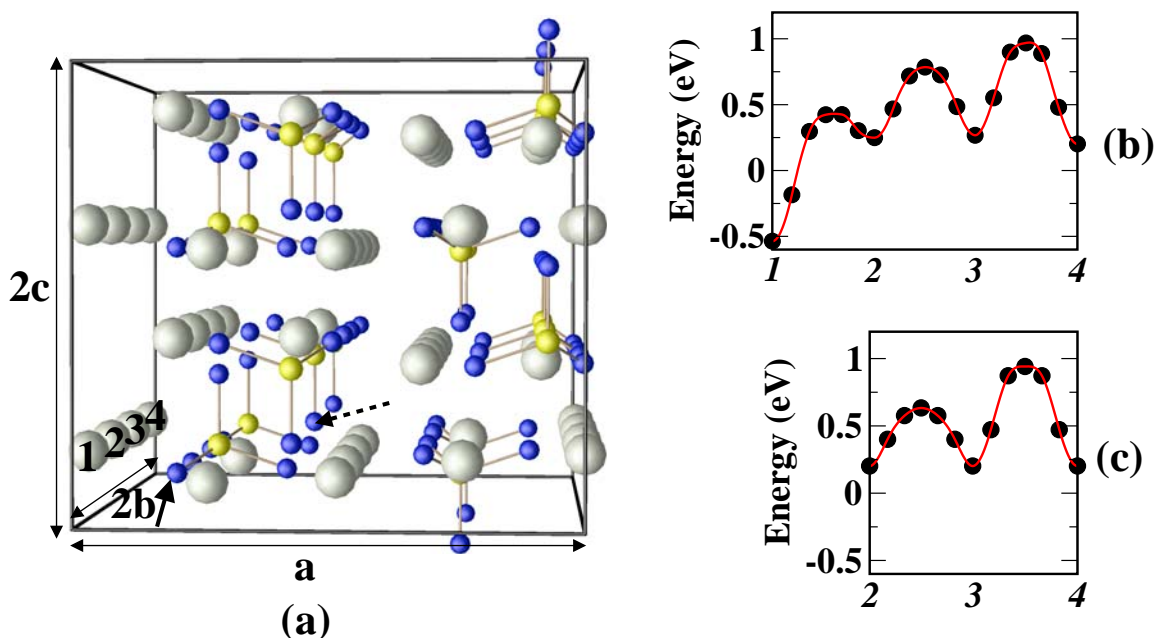


Figure 3. (a) Diagram of the γ -Li₃PO₄ supercell, indicating Li sites with light spheres and tetrahedrally bonded PO₄ groups with smaller spheres and connecting bonds. The **a**, **b**, and **c** axis labels are the same as used in our previous work (7). The large solid and dashed arrows point to the O sites that are removed and replaced with N, respectively, to form the bent PNP structure. The Li site labels 1-4 correspond to the migration path sites. (b) Energy path diagram for vacancy locations 1-4 in the bent PNP structure. The zero of energy is taken so that the vacancy at site 4 corresponds to the similar energy path diagram in bulk γ -Li₃PO₄ which is shown in plot (c).

Simulation of defects which stabilize interstitial Li ions

It is also interesting to consider the formation of extrinsic interstitial Li ions. In these materials, interstitial Li ions are most conveniently stabilized by replacing a phosphate O with N. We studied supercells based on the stoichiometry Li_{3+1/16}PO_{4-1/16}N_{1/16} in which for every 16 formula units of Li₃PO₄ one oxygen ion is replaced with nitrogen, and one Li

ion is added. For $\gamma\text{-Li}_3\text{PO}_4$, the most stable interstitial position (I_0) for an interstitial Li ion was found within a void channel along the c -axis which was found to remain stable in the presence of N substitution. We considered several possible geometries of the N substitution relative to the I_0 site as shown in Fig. 4(a). The corresponding energy path diagrams are shown in Fig. 4(b-c), calculated for the interstitialcy mechanism. We find that the migration energy of hops of the Li ion near the N site, such as the $I_0^1 \leftrightarrow I_0^2$ step for the “A” geometry, have much lower energy than those further away from the N site, so that the N substitutions while stabilizing the Li interstitial ions, also provide traps for them. The migration energy results for the interstitial ion diffusion steps assuming an interstitialcy mechanism are summarized in Table III.

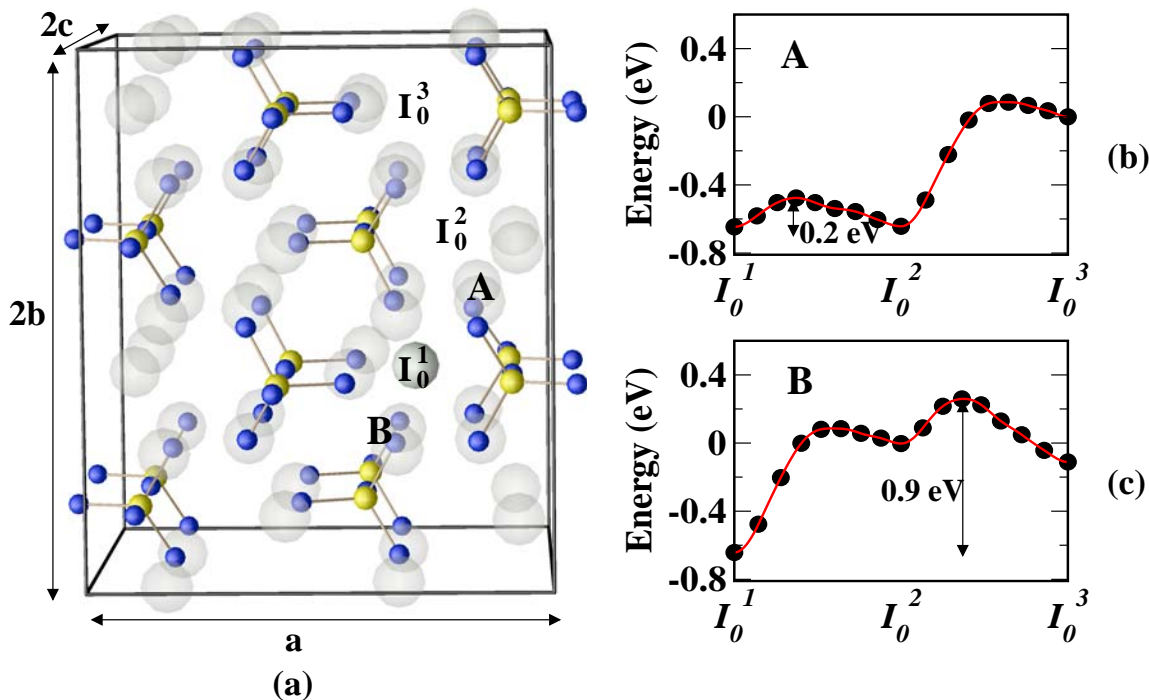


Figure 4. (a) Diagram of the $\gamma\text{-Li}_3\text{PO}_4$ supercell, indicating Li sites with translucent light spheres and tetrahedrally bonded PO_4 groups with smaller spheres and connecting bonds, oriented to show the c -axis void channels which stabilize the interstitial I_0 sites. The labels A and B indicate different O sites for N substitution corresponding to the energy path diagrams (b) and (c). The zero of energy in these diagrams was adjusted so the energy of the I_0^3 site in the A configuration is consistent with that of the corresponding I_0 site calculated for the bulk $\gamma\text{-Li}_3\text{PO}_4$ supercell (7).

Summary and Conclusions

The results of this study have found several structures of isolated defects associated with extrinsic Li ion vacancies and interstitials in crystalline Li_3PO_4 . In particular, we find that O vacancies cause the rebonding of two adjacent PO_4 groups which can be further optimized by replacing the bridging $-\text{O}-$ with a bridging $-\text{N}-$ to form stable bent and straight PNP structures, stabilizing Li ion vacancies. On the other hand, placing a substitutional N within a tetrahedral phosphate group to form PO_3N stabilizes interstitial Li ions in these structures. In both of these cases, the localized defect while providing

sources of mobile Li ions also tends to trap the mobile ions near the defects. Table III summarizes some of the results we have determined so far. In general we find that the migration energies for hops between metastable states of the mobile ions near the defect are comparable or smaller than the corresponding migration energies in the bulk material (7), but larger migration barriers are involved with the ion escaping from the defect region. (The **b**-axis results presented in Fig. 3 are not a good example of this, since vacancy site 2 is already quite far from the O vacancy and thus are not quoted in Table III.) The qualitative differences between migration steps near and far from defect structures provide a possible explanation of the measured activation energies. Wang and co-workers (3) found a doped polycrystalline material with the stoichiometry of $\text{Li}_{2.88}\text{PO}_{3.73}\text{N}_{0.14}$ to have a fairly large activation energy (0.97 eV) which might be attributed to trapping mechanisms similar to those modeled in our simulations. By contrast, LiPON films have been found (1-6) to have much smaller activation energies (0.4-0.7 eV). We expect that in the disordered material, the average environment surrounding mobile Li ions is similar to the vicinities of defect regions modeled in our simulations, so that the most probable migration energies are more similar to those listed in the “defect region” column of Table III and thus consistent with experimentally measured activation energies.

Table III: Migration energies of Li ions in doped Li_3PO_4

Axis	E_m (perfect crystal) ^a	E_m (defect region)	E_m (total)
a (vacancy)	0.7 eV	0.6 eV ^b	1.0 eV ^b
b (vacancy)	0.7 eV	0.5 eV ^c	1.5 eV ^b
c (vacancy)	0.7 eV		1.2 eV ^b
a (interstitial)	0.4 eV		
b (interstitial)	0.3 eV	0.2 eV ^d	0.9 eV ^d
c (interstitial)	0.3 eV	0.2 eV ^d	0.9 eV ^d

^aRef. 7^bSimulations for Li vacancy and bent PNP defect^cSimulations for Li vacancy and straight PNP defect^dSimulations for interstitial Li and substitutional N

Acknowledgments

This work was supported by NSF grants NSF DMR-0405456, DMR-0427055, and DMR-0705239 and benefited from discussions with Xiao Xu at Wake Forest University, as well as from helpful advice from Dr. Nancy J. Dudney of Oak Ridge National Laboratory. Computational results were obtained using the DEAC cluster, and benefited from storage hardware awarded to Wake Forest University through an IBM SUR grant.

References

1. J. B. Bates, N. J. Dudney, G. R. Gruzalski, *et al.*, *Solid State Ionics* **53–56**, 647 (1992).

2. J. B. Bates, N. J. Dudney, G. R. Gruzalski, *et al.*, *Journal of Power Sources* **43–44**, 103 (1993).
3. B. Wang, B. C. Chakoumakos, B. C. Sales, *et al.*, *J. Solid State Chem.* **115**, 313 (1995).
4. X. Yu, J. B. Bates, J. G. E. Jellison, and F. X. Hart, *J. Electrochem. Soc.* **144**, 524 (1997).
5. Y. Hamon, A. Douard, F. Sabary, *et al.*, *Solid State Ionics* **177**, 257 (2006).
6. W.-Y. Liu, Z.-W. Fu, C.-L. Li, and Q.-Z. Qin, *Electrochemical and Solid-State Letters* **7**, J36 (2004).
7. Y. A. Du and N. A. W. Holzwarth, *Phys. Rev. B* **76**, 174302 (2007), Y. A. Du and N. A. W. Holzwarth, *J. Electrochem. Soc.* **155**, A999 (2007).
8. P. Hohenberg and W. Kohn, *Phys. Rev.* **136**, B864 (1964); W. Kohn and L. J. Sham, *Phys. Rev.* **140**, A1133 (1965).
9. J. P. Perdew and Y. Wang, *Phys. Rev. B* **45**, 13244 (1992).
10. S. Baroni, A. D. Corso, S. de Gironcoli, P. Giannozzi, C. Cavazzoni, G. Ballabio, S. Scandolo, G. Chiarotti, P. Focher, A. Pasquarello, *et al.*, available from the website <http://www.pwscf.org/>.
11. D. Vanderbilt, *Phys. Rev. B* **41**, 7892 (1990); the USPP code is available from the website <http://www.physics.rutgers.edu/~dhv/uspp/>.
12. H. J'onsson, G. Mills, and K. W. Jacobsen, in *Classical and Quantum Dynamics in Condensed Phase Simulations*, edited by B. J. Berne, G. Ciccotti, and D. F. Coker (World Scientific, Singapore, 1998), pp. 385–404.
13. G. Henkelman, B. P. Uberuaga, and H. J'onsson, *J. Chem. Phys.* **113**, 9901 (2000).
14. G. Henkelman and H. J'onsson, *J. Chem. Phys.* **113**, 9978 (2000).
15. A. K. Ivanov-Shitz, V. V. Kireev, O. K. Mel'nikov, and L. N. Demainets, *Crystallogr. Rep.* **46**, 864 (2001).